Geophys. J. R. astr. Soc. (1975) **42,** 747–768.

The Application of Finite Element Analysis to Body Wave Propagation Problems

Warwick D. Smith*

(Received 1974 October 1)

Summary

The finite element method is shown to be a powerful tool for the numerical modelling of seismic body wave propagation problems. Applications extend to both problems on a scale of interest to engineers and also to large-scale seismological problems. Solutions are sought in the time domain. Efficient programs have been written to accomplish this. The scope of numerical solutions has been greatly enhanced by the use of a previously reported scheme for exactly cancelling reflections at the boundaries of the model.

The finite difference results of Boore and the analytical results of Trifunac for the amplification due to a mountain and an alluvial valley respectively are compared with new finite element results. The new results agree well, although there are some difficulties with resonance in the alluvial valley problem. Boore's *SH* results have been extended to vertical *P* and *SV* incidence. A deep earthquake zone has been modelled realistically in two dimensions and earthquakes simulated at depth. It is suggested that the variation in observed amplitude across the top of the zone, due to refraction away from the slab, may be used to provide an estimate of the thickness of the slab from long-period observations of local earthquakes.

1. Introduction

Only simple wave propagation problems can be solved analytically. Material properties may be allowed to vary throughout the model, but generally only in the vertical (or radial) direction. The presence of lateral variation often renders the solution intractable. Certain classes to scattering problems admit analytical solutions, but the restriction to regular geometries is generally very severe (e.g. Trifunac 1971). Analytical approaches that are concerned with the scattered energy do not apply in the near field or when the wavelengths of the irregularity and the incident energy are comparable.

Irregular geometries and inhomogeneous media that represent realistic geological structures must generally be analysed by numerical means, and approximate solutions sought. Traditionally, this has meant recourse to a finite difference scheme. The governing differential equations are replaced by difference equations, which are then solved numerically. Recent work in seismology using this approach is by Boore (1972a), Alterman & Karal (1968), and others. But the Ritz method, in which a

* On leave from: Geophysics Division, Department of Scientific and Industrial Research, P.O. Box 8005, Wellington, New Zealand.

solution is sought in terms of known functions, has equally deep roots in the applied mathematical literature. Courant (1943) made an able comparison of the two techniques. A particular application of the Ritz method is the finite element method, which is now widely used in many applications in engineering, and is emerging as a seismological tool. Particular efforts in this direction have been made at the Seismographic Station, Department of Geology and Geophysics, University of California, Berkeley. In this paper the applicability of the finite element method to body wave propagation problems is examined.

Only one aspect of finite element applications to seismology is treated: that of the time domain solution of body wave propagation problems. Time-dependent problems can sometimes be treated in the frequency domain, notably the propagation of surface waves (e.g. Lysmer & Drake 1972), but this technique is applicable to body waves only in very special cases. Nor does this paper treat source theory, although finite element methods certainly can be applied (e.g. Glover, McCowan & Alexander 1975). It is confined to the effects of the medium on the propagation of *P* and *S* waves. The geophysical purpose is to demonstrate that the finite element method is a powerful tool for determining the effect of structural irregularities on wave propagation.

Three problems of seismological importance are discussed. The first two concern the ground amplification which is observed in the presence of topographic or geologic irregularities, in this case a mountain and an alluvial valley. Numerical results of Boore (1972b) and theoretical results of Trifunac (1971) for incident *SH* waves have been duplicated and the former extended to incident *P* and *SV*. The third problem that is presented is that of determining the structure of a deep earthquake zone. The New Zealand North Island seismic zone has been modelled in two dimensions, and earthquakes simulated at a depth of 250 km. Theoretical seismograms written at the surface reflect the structure of the zone to a measurable extent, and it is suggested that such a technique could lead to the determination of such structural parameters as the thickness of the dipping slab, within which the earthquake foci are located.

2. The finite element method and its implementation

(a) *Formulation*

A number of texts present the basic formulation of the finite element method, e.g. those by Zienkiewicz (1971), Desai & Abel (1972), Norrie & de Vries (1973) and Lysmer & Drake (1972). Though the first three are written with engineering applications in mind, the overlap with seismology is adequate. A brief outline of the technique and terminology is all that is necessary here.

Each *element* of the model has (usually at its extremities) a number of *nodes*, at which the elastic displacements are to be determined. In Fig. 1 the two-dimensional element shown is a quadrilateral, with a node at each vertex and, in this case, two components of displacement at each node. (For *SH* motion there will be only one component.) Two adjacent elements share the nodes on their common boundary. From a variety of elements that can be used, the element shown in Fig. 1 has been chosen as the basic element for the applications presented in this paper. Displacements within the element are linearly interpolated from the values at the nodes. The isoparametric interpolation formulae are given by Lysmer & Drake (1972). (The term 'linear element' is used in the finite element literature when such interpolation is employed.) Herein lies the basic assumption of the technique, and it is at this point

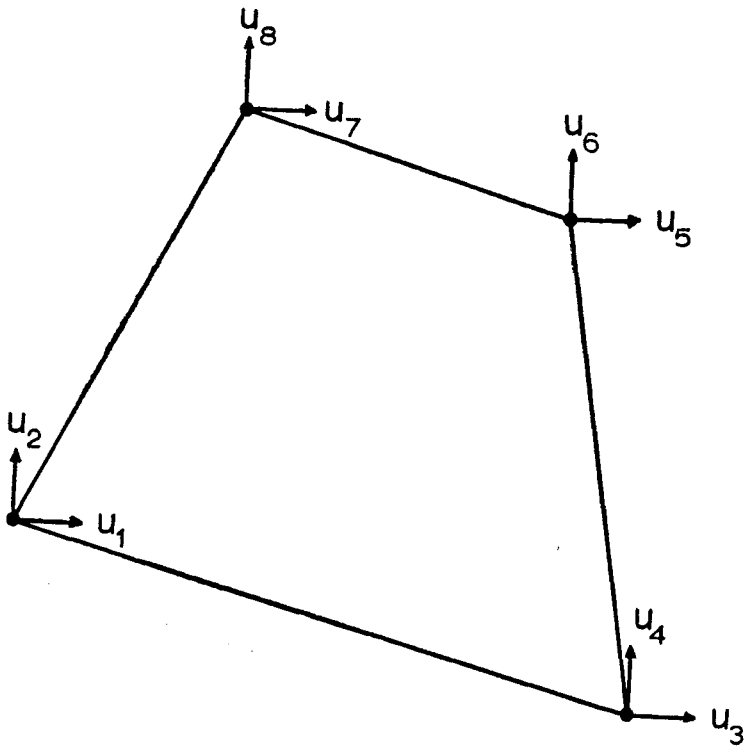

FIG. 1. Basic finite element used in this paper. The quadrilateral has four nodes and two components of displacement at each node. Thus the displacement vector **u** has eight components.

that the degree of approximation must be carefully evaluated. This point will be given further attention in Section 2(d).

The elastic and dynamic relations between the displacements at the nodes of the element may be expressed in terms of a *stiffness matrix* $\boldsymbol{K}^e$ and a *mass matrix* $\boldsymbol{M}^e$. If the components of displacement are written as a vector $\mathbf{u}^e$ ($\mathbf{u}^e$ has eight terms for the element in Fig. 1), then the equation of motion for the element takes the form

$$\boldsymbol{M}^e \ddot{\mathbf{u}}^e + \boldsymbol{K}^e \mathbf{u}^e = 0. \tag{1}$$

A dot denotes differentiation with respect to time. Both matrices are real, symmetric, and positive definite. They may be computed for each element independently, and accumulated into global matrices $\boldsymbol{K}$ and $\boldsymbol{M}$, so that, where $\mathbf{u}$ now represents all the displacement components in the entire model,

$$\boldsymbol{M}\ddot{\mathbf{u}} + \boldsymbol{K}\mathbf{u} = 0. \tag{2}$$

A forcing term $\mathbf{F}$ and/or a damping term $\boldsymbol{C}$ may also appear.

$$\boldsymbol{M}\ddot{\mathbf{u}} + \boldsymbol{C}\dot{\mathbf{u}} + \boldsymbol{K}\mathbf{u} = \mathbf{F}. \tag{3}$$

It is then necessary to solve this set of differential equations, with appropriate initial conditions and boundary conditions. All the geometrical and elastic properties of the model are taken into account in the construction of the three matrices $\boldsymbol{K}$, $\boldsymbol{C}$ and $\boldsymbol{M}$, and the load vector $\mathbf{F}$. The matrices are very large and so require considerable computer storage. They are however very sparse, and may be condensed very efficiently. The Appendix gives details of how this has been done.

(b) *Frequency domain solutions*

Time dependent finite element calculations are often performed in the frequency domain. Equation (3) becomes

$$(\boldsymbol{K}+i\omega\boldsymbol{C}-\omega^2\boldsymbol{M})\,\mathbf{u} = \mathbf{F}. \tag{4}$$

where ω is the angular frequency. The displacements $\mathbf{u}$ and the load vector $\mathbf{F}$ are now complex. This approach is appropriate for certain applications with surface waves (e.g. Drake 1972a, b), or for body waves when the scale of the problem is much less than the exciting wavelength (e.g. Lysmer, Seed & Schnabel 1971). It is not appropriate for body wave propagation problems with wavelengths shorter than the scale size. In these cases it is necessary to solve equation (3) in the time domain.

(c) *Numerical implementation*

The matrix $\boldsymbol{M}$ above is the so-called consistent mass matrix. In its place I have used the lumped mass matrix, which is an approximation to the consistent mass matrix, and is diagonal in form. It has been well established in the finite element literature (e.g. Clough 1971) that the lumped mass matrix is to be preferred to the consistent mass matrix, for wave propagation problems in the time domain. Equation (3) may therefore without difficulty be cast into the form

$$\ddot{\mathbf{u}} = \boldsymbol{M}^{-1}(\mathbf{F}-\boldsymbol{K}\mathbf{u}-\boldsymbol{C}\dot{\mathbf{u}}). \tag{5}$$

In this form the equation is amenable to numerical solution by a Runge-Kutta algorithm (e.g. Abramowitz & Stegun 1970; Carpenter & Gill 1973), which has the advantage that it is explicit; the calculation requires only multiplication of matrices and vectors, and addition of vectors, so it is very efficient. It also has the advantage that it is self-starting, and this makes it particularly easy to program.

It is important to note the distinction between explicit and implicit schemes. The Newmark method (Newmark 1959), is widely used in engineering applications of the finite element method but it has the disadvantage that it is implicit (except for the particular case when the parameter β is zero) and thus involves the solution of linear equations at each time step. The computing effort in such a scheme would seem to be unnecessarily great, especially since cost is one of the chief considerations for finite element calculations. A further advantage of explicit computation schemes is that non-linear stress-strain relations can be incorporated without difficulty. This has not been attempted here, but it should be appreciated that if an implicit scheme were used iteration at each step would be necessary.

The mesh can be excited either through the forcing function $\mathbf{F}$ or by defining initial displacements and velocities. The latter option has been chosen. For plane wave excitation, the nodes on the boundary are given a small displacement for a short time, then returned to their initial positions. For a point source, this is done only at the node in question. For P or SV motion, as with the element in Fig. 1, the choice of displacement component to be excited determines the type of wave that will propagate. Nodes at which the excitation is applied are held rigid by the device of setting to zero the corresponding terms of the inverted mass matrix $\boldsymbol{M}^{-1}$. This effectively sets infinite mass at these points and prevents motion there.

The pulse propagates throughout the mesh and can be observed at any desired locations. The response of the model to any other input may then be obtained by convolution. Alternatively, results may be obtained in terms of spectral ratios: spectra are taken at two or more locations, and their ratios formed. This ratio will thus be independent of the source function, and describes the response at one location relative to that at another.

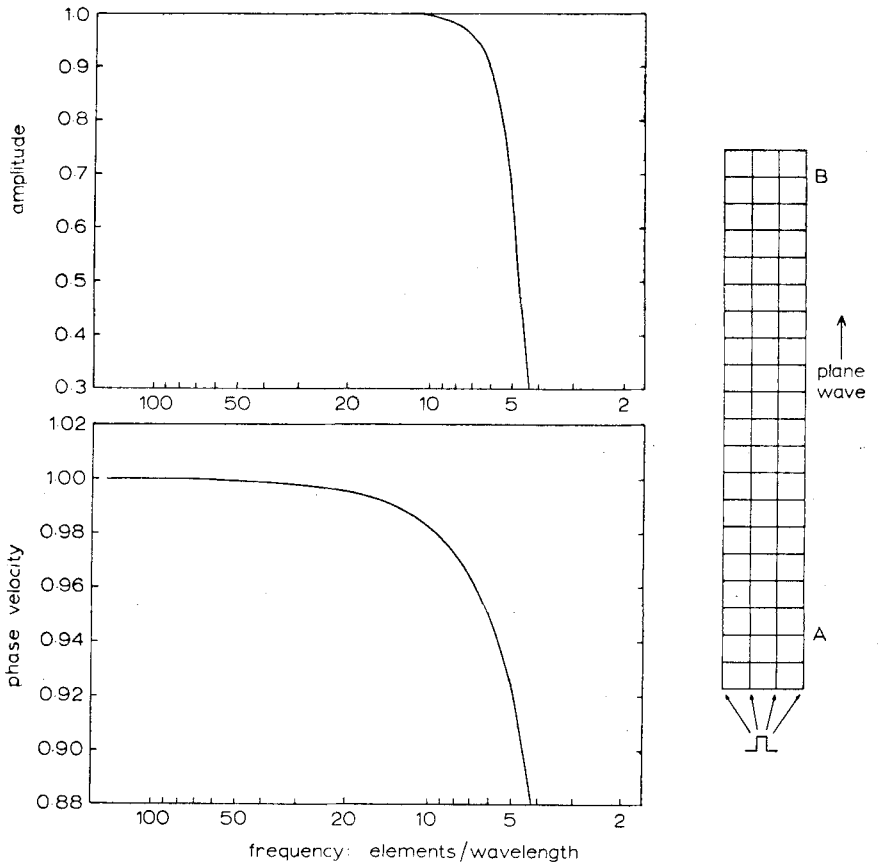

FIG. 2. Attenuation and dispersion characteristics of a mesh, determined by propagating a pulse along the bar model shown at right.

(d) *Mesh design*

The size of elements is a critical consideration in all finite element calculations. In wave propagation problems the error introduced by elements that are too large will be a function of wavelength. Wavelengths shorter than the element length will obviously not be properly accounted for if interpolation between adjacent nodes is linear. To examine the frequency characteristics of a mesh, the model shown at the right of Fig. 2 was used: a pulse was applied at the base and allowed to propagate as a plane wave. The technique referred to in Section 2(e) was used to eliminate reflections at the upper end. The ratio of the spectra of displacements at A and B gives a measure of the propagation characteristics between the two points. Amplitude gives attenuation information and dispersion can be found from the total phase. These data are shown in Fig. 2, for a path 1 km long. Frequency has been shown as the ratio of wavelength to element size. Both the amplitude and the phase velocity have been normalized. It is clear that at 10 elements per wavelength attenuation is negligible and dispersion is limited to about 1 per cent. At eight elements per wavelength the attenuation and dispersion are about 3 per cent each, and this figure was considered adequately small. The amount of computer storage available will influence the choice of element size and the scope of problems that can be attempted. Eight elements per wavelength seems to be a reasonable compromise between economy of storage and accuracy of solution.

It should be emphasized that the attenuation and dispersion curves of Fig. 2 apply to one-dimensional propagation through linear, rectangular elements. Irregular elements, high order elements, or curved wavefronts will naturally affect the frequency characteristics. Moreover, the curves relate to the particular time-stepping algorithm (fourth order Runge-Kutta) and to the length of time step that was used. Decreasing the time step improves the amplitude curve a little (i.e. larger elements may be used). It does not appear to affect the dispersion. Furthermore, the amplitude curves depend on length of propagation path. Attenuation is approximately exponential with distance, if it is small, but is rather greater than exponential for very high frequencies. In spite of the inadequacies of the test illustrated in Fig. 2, the figure of eight elements per wavelength was taken as a working standard, and the finite element model laid out accordingly. This agrees with the result of Kuhlemeyer & Lysmer (1973). On intuitive grounds it is not unreasonable, since one cycle of a sine wave may be quite well modelled by eight line segments.

(e) *Non-reflecting boundaries*

With infinite fields it is always necessary to introduce fictitious boundaries into the model. It is highly desirable to be able to eliminate reflections at these boundaries, because they would otherwise contaminate the solution. A technique which exactly cancels such reflections has been developed, and has been reported elsewhere (Smith 1974). At the heart of the scheme is the principle that if two independently calculated solutions in which the reflections are of opposite sign are added together, the reflections exactly cancel, leaving only the energy originally incident on the boundary. An infinite medium has thus been simulated. The two solutions correspond to the application of homogeneous Dirichlet and Neumann boundary conditions respectively. The formulation is appropriate for body waves in two or three dimensions, and for surface waves. There is a special difficulty that arises in cases of plane wave excitation. This is dealt with in Section 3.

(f) *The question of damping*

Shipley, Leistner & Jones (1967) examined the accuracy of finite element solutions and found a ringing phenomenon which dies away only gradually. The frequency of this oscillation is related to the size of the elements used. It may perhaps be best understood by reference to Fig. 2. At frequencies of about 4–6 elements per wavelength the phase velocity falls off very sharply with increasing frequency. The group velocity will thus behave in a similar fashion, with the result that there will be a train of dispersed energy following the main pulse.

Efforts to suppress this ringing have generally been by way of added damping. Wilson (1969) constructed a damping matrix $\boldsymbol{C}$ (see equation (3)) from a linear combination of the stiffness matrix and the mass matrix. The use of the mass matrix (or some proportion thereof) as a damping matrix results in attenuation that is independent of frequency, and this is of no use in reducing the ringing. Some proportion of the stiffness matrix, used for damping, does indeed strongly damp out the ringing, because the damping that is introduced is proportional to the square of the frequency. That is, it introduces a Q that is inversely proportional to frequency.

I have preferred to retain the perfectly elastic formulation, and to try to continue the solution for a sufficient time until the ringing has died down. The frequencies present in the ringing are higher than can be accurately computed, so the elastic solution should contain all the necessary information when examined in the frequency domain, i.e. by first taking the Fourier spectrum. For examination in the time domain, traces may be low-pass filtered with a suitable numerical filter, and the ringing removed.

The ringing may be reduced, however, even in the perfectly elastic case, by careful choice of the length of the exciting pulse. A square pulse has a spectrum of the form $\sin \alpha f/f$, where f is the frequency and α a constant. Diminished ringing results if the pulse length is chosen so that the first zero in the spectrum corresponds to the ringing frequency. A poorer approximation to an impulse source function is the price that is paid.

3. The effect of simple topography on ground amplification in earthquakes

Following the San Fernando earthquake of February 1971, there was much interest in the question of amplification of ground motion by surface topography. Boore (1972b) showed that *SH* motion can be significantly amplified by the presence of a mountain, which he modelled in two dimensions. In subsequent work (Boore 1973), he has attempted to model the Pacoima Dam topography more realistically. He concludes that amplification was probably significant at the higher frequencies but was relatively unimportant at lower frequencies. Field observations (e.g. Davis & West 1973) and model studies (e.g. Rogers, Katz & Bennett 1974) tend to support the conjecture that topography can play an important role. Reimer (1973) has attempted to model the Pacoima site using three-dimensional finite elements, with an analysis in the frequency domain. His results are of limited applicability, however, because he applied equal excitation, in phase, along the base of his model and to all vertical side faces.

It is beyond the scope of this paper to examine the Pacoima geometry, or any other, in detail. Rather, it will suffice to show simply how the finite element method may be usefully applied to this type of problem. The analysis will be restricted to two dimensions. There is no difficulty in programming the three-dimensional case, but the computer storage required makes it impracticable with currently available facilities. Fig. 3 shows the finite element model that was used to duplicate Boore's (1972b) results. The sides of the mountain slope at 20° to the horizontal; the material is homogeneous. A displacement pulse was applied along the entire base, and allowed to propagate up to the surface as a plane wave.

The technique for elimination of reflections (Section 2(e)) does not allow propagation parallel to a non-reflecting boundary. This is because it involves the addition of two solutions in which reflections are of opposite sign. The negative reflection is achieved for *SH* propagation by setting to zero the boundary displacements, and this will distort the plane wave as it propagates along the end boundaries. Positive reflections are achieved by allowing boundary displacements to move freely, and it is this condition that allows plane waves to propagate undistorted. It is therefore necessary not to attempt to cancel at the ends of the model the reflection of energy that has radiated out from the topographic irregularity, but to build the model wide enough that the desired solution can be obtained before reflections from the ends arrive. Reflections from the base can be cancelled without difficulty.

Similar considerations apply to *P* wave propagation, except that the horizontal displacements must be held to zero at the ends of the model to ensure plane wave propagation. For *SV* the vertical displacements must be held rigid. These conditions imply positive and negative reflections respectively at the ends of the model, and no conversion from *P* to *SV* or vice-versa (Smith 1974).

Theoretical seismograms can be observed at any desired locations. Fig. 4 shows these seismograms, together with a location diagram for the observing sites. The problem is clearly symmetric in the case of vertical incidence, so only one side of the mountain need be observed. The ringing mentioned in Section 2 has been removed by low-pass filtering. These seismograms approximate the impulse response at the

FIG. 3. Schematic model of a mountain, used to investigate the effect on energy vertically incident from below. A pulse is applied at the base, and it propagates up to the surface as a plane wave. See Fig. 4 for dimensions.

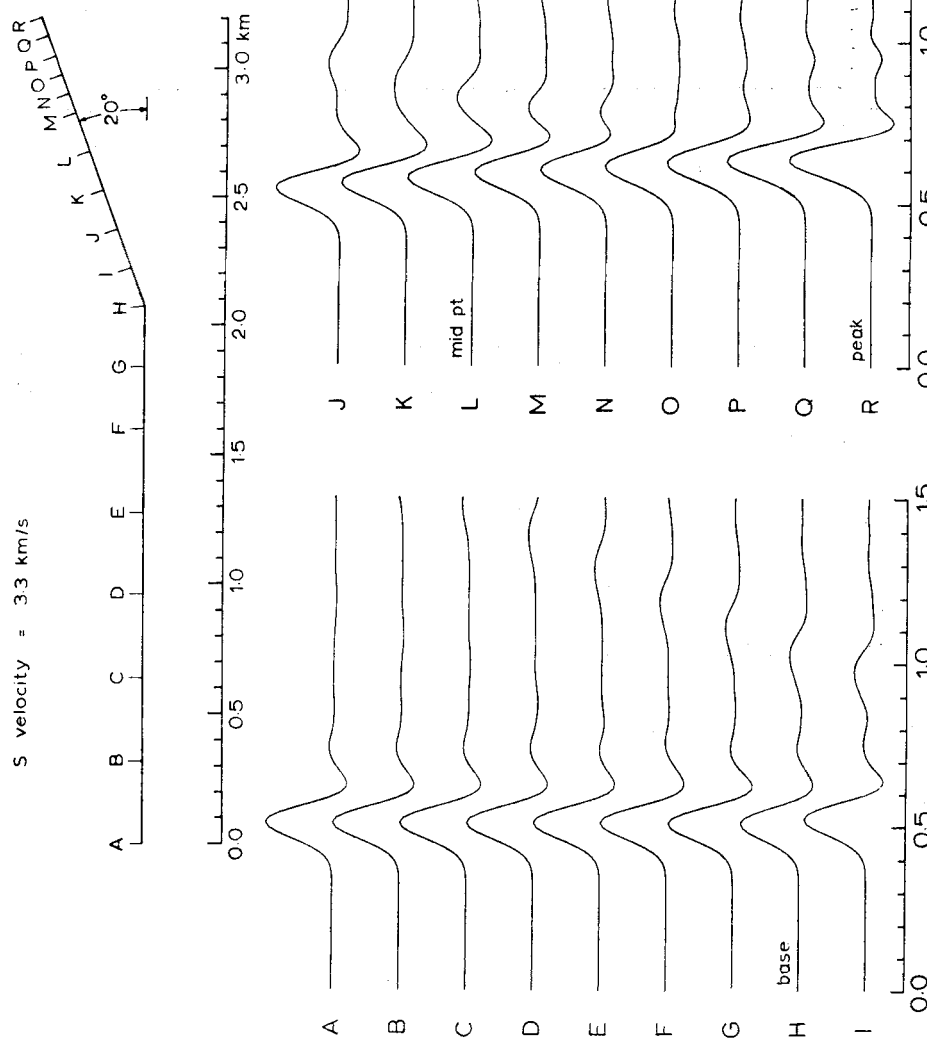

FIG. 4. Displacements observed at various sites on and near the mountain. These traces approximate the impulse response at each location.

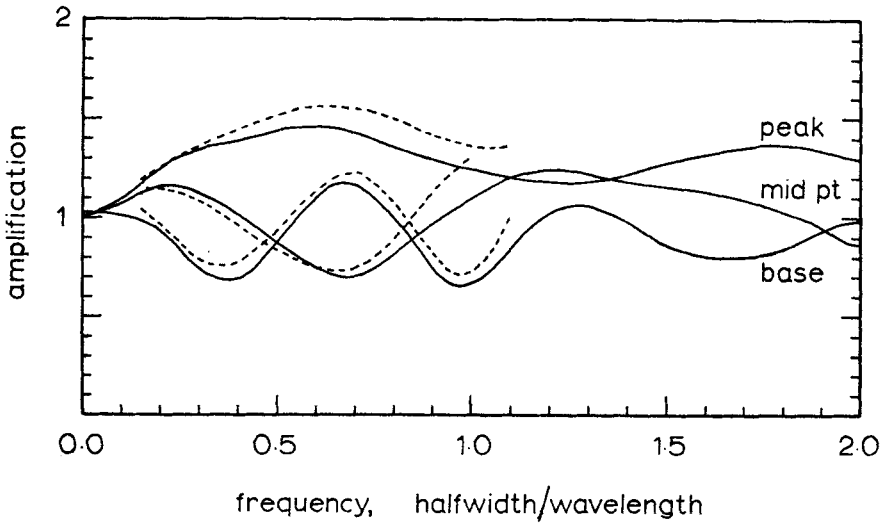

FIG. 5. Fourier spectra of the *SH* traces in Fig. 4 for the base, mid-point and peak of the mountain. The broken curves at each location are the finite difference results of Boore (1972).

different locations for *SH* energy vertically incident from below. Of interest is the diffracted pulse that propagates away from the mountain and can be seen following the main pulse.

In order to determine the amplification due to the mountain, the source function may be removed by taking the Fourier spectra of the traces in Fig. 4, and dividing by the spectrum that is obtained in the absence of the mountain. This is shown in Fig. 5 for these locations: the base, the midpoint of a side, and the peak. Also shown are Boore's (1972b) results for his equalent locations. Dimensionless frequency is given by the ratio of the half-width of the mountain to the wavelength. The analytical value of 1·0 at zero frequency is reproduced to within a few per cent.

The spectra for vertical *P* incidence appear in the upper half of Fig. 6, at the same three locations. The lower plot shows the *SV* results. There are now two components of motion at each location, and of course now no previous results for comparison. Significant is the amplitude observed on the horizontal component at the peak of the mountain for *SV* incidence, which reaches a maximum of 1·8. Amplification due to *P* incidence reaches a maximum of 1·2. The base of the mountain experiences attenuation at most frequencies, and the peak experiences mostly amplification. Further study with realistic geometry and geology will be needed to fully resolve the Pacoima question in a quantitative way. It may even need three-dimensional analysis.

4. Ground amplification due to near-surface geology: problems with resonance

Closely akin to the problem of the previous section is that of the local variation in ground motion observed in an earthquake, due to the underlying geological structure. Trifunac (1971, 1972) has treated analytically the two-dimensional problem of plane *SH* waves incident at arbitrary angles on a semi-cylindrical alluvial valley. His treatment is in the frequency domain. He shows the variation across the valley at particular frequencies, and the amplification at one particular location, as a function of frequency. The purpose of this section is to attempt to repeat Trifunac's calculations for *SH* using the finite element method.

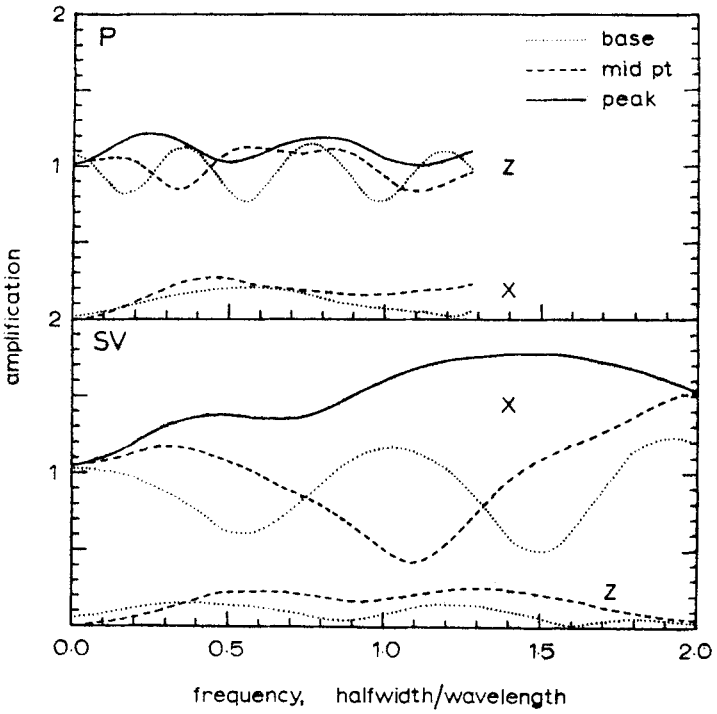

FIG. 6. Fourier spectra at the same locations as in Fig. 5, for *P* and *SV* incidence. There are now two components of motion at each location. *Z* indicates the vertical component, and *X* the horizontal component.

The technique is the same as that of the previous section, in that a plane pulse is incident from below. The seismograms written at specified locations are examined by taking spectra. The model is shown in Fig. 7; because the geometry is symmetric about the centre of the valley, only half the model need be drawn. For the *SH* problem the axis of symmetry is taken as a free surface. Reflections occurring there are exactly those of the image propagation, and so the complete model may be simulated. This may also be achieved for *P* incidence by demanding that there be no horizontal displacement along the axis. This boundary condition can be shown (Smith 1974) to result in no mode conversion from *P* to *SV* or vice-versa at the boundary, and reflection in the proper phase. This cannot be done for the *SV* problem, however, since fixing the horizontal displacements would distort the original plane wave. The complete model would therefore need to be used for the *SV* case, and with this in view a facility for constructing the image grid was built into the program.

A square pulse was applied at the base of the model, as in Section 3, and was observed at the surface. Fig. 8 shows the seismograms for the *SH* case, at various locations from the centre of the valley to its rim, and slightly beyond. The resonance that takes place is important: reflected pulses can be seen at all locations in the valley.

Trifunac (1971) calculated the amplification as a function of frequency for one particular location, at a distance of $0{\cdot}8r$ from the centre, where r is the valley radius. He used a velocity in the valley of one half that outside, and a density two thirds the outside value. These parameters have been retained. His results have been reproduced in Fig. 9, together with the finite element spectrum calculated from Fig. 8 and expressed as spectral ratios as was done in Section 3. The frequency is in dimensionless units.

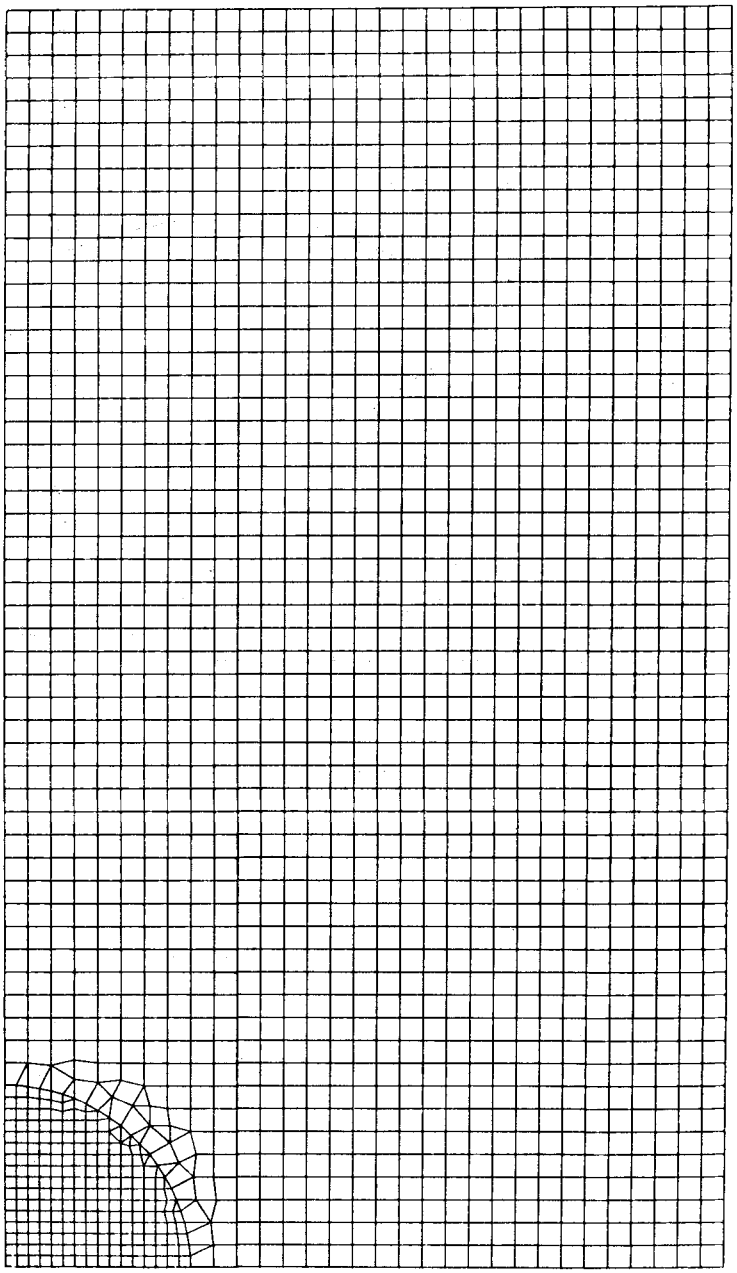

FIG. 7. Representation of a cylindrical alluvial valley by finite elements. Smaller elements are used in the valley, where the velocities are less. The model is 2·5 km high. *S* velocity and density are 2·0 km s^{-1} and 2·50 g cm^{-3} outside, 1·0 km s^{-1} and 1·67 g cm^{-3} inside.

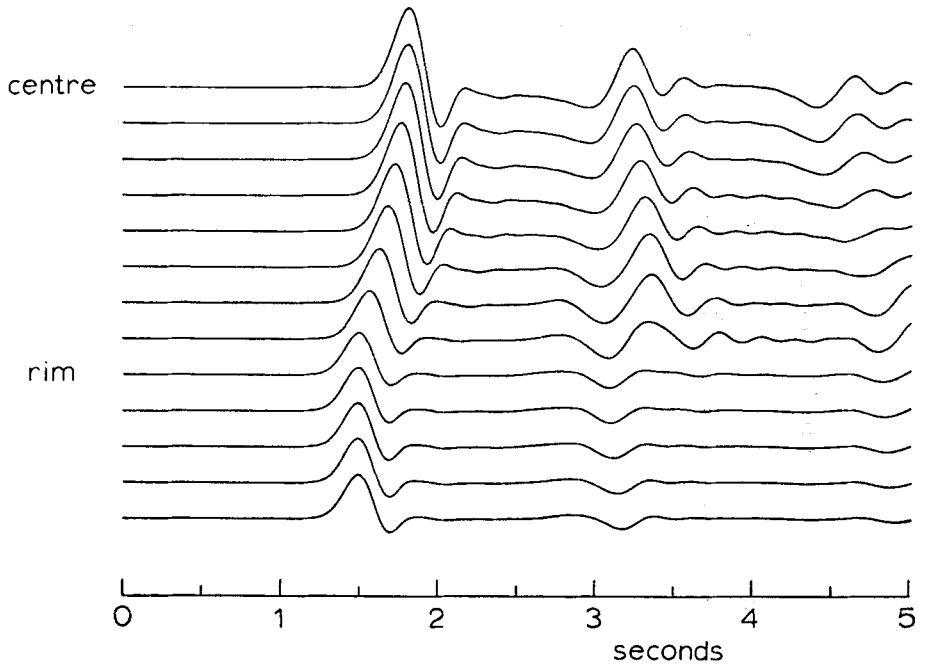

FIG. 8. Displacements observed in and near the valley. These traces approximate the impulse response at each location.

The discrepancy between the analytical and finite element results is clearly due to the short time window that has been used. The seismograms of Fig. 8 are unable to completely characterize the resonance because their duration is too short. The finite element spectrum of Fig. 9 represents only the first two reflections in the valley so it is not surprising that the fit to the analytical result is not exact. But it does illustrate the problem which must be faced when resonance occurs. The grid must be constructed large enough that reflections from the ends or multiple reflections from the base will not force truncation of the signal before the solution is complete. The sharp peaks in Trifunac's analytical results demand a long time window in order to obtain the necessary resolution in the frequency domain.

Trifunac's results could have been extended to *P* and *SV* incidence, as in the previous section, but limitations imposed by resonance render this exercise somewhat pointless without the construction of a much larger grid.

Clearly the solution to any practical problem will involve both this section and the previous one, i.e. both topography and geology will have an effect. An attractive feature of the finite element method is that inhomogeneous models may be constructed very easily (e.g. Douglas 1970), since the matrices are built up one element at a time. Incidence at angles other than vertical could be accomplished in several ways. The input pulse could be stepped along the base at the appropriate apparent velocity. Alternatively, a new model could be constructed with the free surface inclined to the base at the required angle. A further approach would be to set up the displacement and velocity fields of the incident wave, and then let it propagate. This is perhaps the most general technique. It is the one used, for example, by Boore (1972b) in his finite difference work.

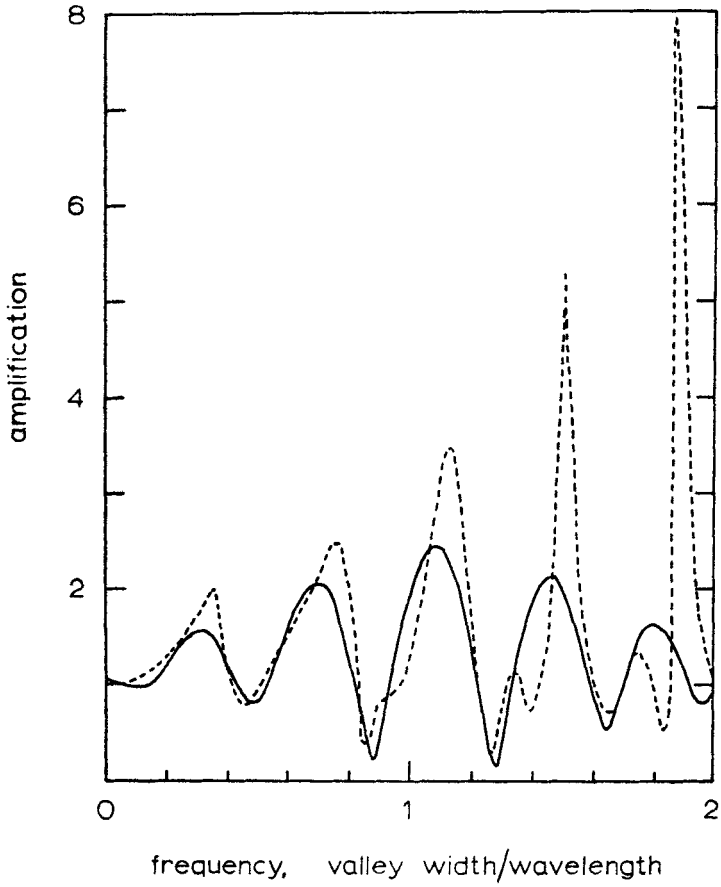

FIG. 9. Fourier spectrum of the *SH* trace in Fig. 8 corresponding to the point $0{\cdot}8r$ from the centre of the valley, where r is the radius. Trifunac's (1971) analytical result is shown by the broken line.

5. Estimation of the structure of a deep earthquake zone

Deep earthquake zones present challenging problems in geophysics. That deep earthquakes usually occur in dipping, almost planar volumes beneath island arcs and at continental boundaries has been known for decades (e.g. Gutenberg & Richter 1949) and this of itself suggests a different velocity structure from the surrounding mantle. Attenuation studies (e.g. Barazangi & Isacks 1971, and refs. therein) support this conjecture, observing that high frequency seismic waves are attenuated much less in the dipping slab than when propagating to stations away from it. Mitronovas & Isacks (1971) inferred that slab velocities in the Tonga-Kermadec region are 6–7 per cent higher than in the surrounding mantle, though this idea was not new (e.g. Davies & McKenzie 1969).

Estimates of the thickness of the slab, however, are quite uncertain, as this is an extremely difficult parameter to measure. Oliver & Isacks (1967) used the expression 'perhaps of the order of 100 km' for the thickness of the Tonga–Kermadec slab, based on attenuation studies. Jacob (1972) inferred a thickness of 80 km for the Aleutian slab, from consideration of *P* residuals from the nuclear explosion Longshot. There is little reason to suppose that this thickness should be the same as that of the

FIG. 10. Finite element representation of a deep earthquake zone. The P velocity (α), S velocity (β) and density (ρ) are shown at left, both in the slab (dashed lines) and in the surrounding mantle (solid lines). The slab is 50 km thick. Displacements due to the earthquake are observed at the indicated locations on the surface.

seismic zone, i.e. the actual envelope of earthquake foci, for which, in the Tonga–Kermadec region, Wyss (1973) inferred a thickness of 11 km, based on considerations of the source dimensions of large earthquakes. The question of the thickness of the seismic zone is one which can perhaps be answered by such considerations of source size or by examination of accurately determined focal positions.

The finite element method can be used to model a deep earthquake zone, and it now appears that such modelling could lead to an estimation of the structural properties of the zone. Fig. 10 shows such a model. On the right can be seen clearly the outline of the slab, with an earthquake focus at a depth of 250 km. On the left is the velocity model that was used, both in the slab (dashed lines) and in the surrounding mantle (solid lines). The procedure is to simulate an earthquake at depth, and from seismograms written at the surface to endeavour to infer the structure of the zone.

The configuration approximates that of the North Island of New Zealand. It is a vertical section, looking north-east. (See Hamilton & Gale 1968.) The restriction to two-dimensional modelling is a limiting one, not as concerns the structure but more particularly with reference to the three-dimensional radiation from earthquakes. This point will be mentioned again later. Some of the stations of the New Zealand seismograph network are in positions comparable to location E in Fig. 10, i.e. they may be said to ' look right down the slab '. The New Zealand region might be almost unique from this viewpoint. The seismograph network is distributed across the top of the zone, so that observation at locations corresponding to the positions A to E in Fig. 10 is quite feasible.

The velocity model is one about which there could be considerable argument. Velocities increase with depth in the slab, and are approximately 7 per cent higher than in the surrounding mantle, following Mitronovas' & Isacks' (1971) result. The velocities in the mantle incorporate an increase with depth to 100 km, then a pronounced low velocity zone for both *P* and *S*. My earlier work (Smith 1973) has been taken into account here, though the published profile has been smoothed somewhat. Mooney (1970a, b) gives further evidence for such velocity structure. A slight density increase has been included for the slab (Hatherton 1970). This model is not to be considered definitive, but rather to represent a feasible structure. The aim of the finite element calculation is to ascertain the extent to which such a structure can affect the seismograms of local deep earthquakes.

The perfectly elastic formulation of the previous sections has been retained. This is clearly a disadvantage, since observations of local earthquakes show a marked dependence on the lateral variation of Q (Mooney 1970a). But, as was outlined in Section 2(f), the damping commonly employed in finite element calculations is not very realistic. In this case it is not too serious to assume perfect elasticity, because the elements that have been used are of such a size (5 km square in the mantle and slab) that they restrict the analysis to periods of 10 s and longer. The commonly observed attenuation effects are for much higher frequencies. An extremely low Q (less than 20 or so) would be needed to see much effect at the surface for these low frequencies, and while in fact Q may be as low as this behind the arc (Barazangi & Isacks 1971), the elastic case does convey important information.

Fig. 11 shows the seismograms for an *SH* source at 250 km, written at the surface locations shown in Fig. 10. The source is a very simple one. It is the same square displacement pulse as was used in the previous sections, but is now applied at a point rather than along a boundary face. No secondary arrivals due to reflection in the slab or low velocity zone can be distinguished, because of the lack of high frequencies in the signal. The amplitude at E is considerably less than at A. This is opposite to the attenuation effect observed at high frequencies, and occurs because energy refracts away from the high velocity slab.

The amplitude variation across the top of the deep earthquake zone may provide a means of estimating such structural parameters as the thickness of the slab. Further

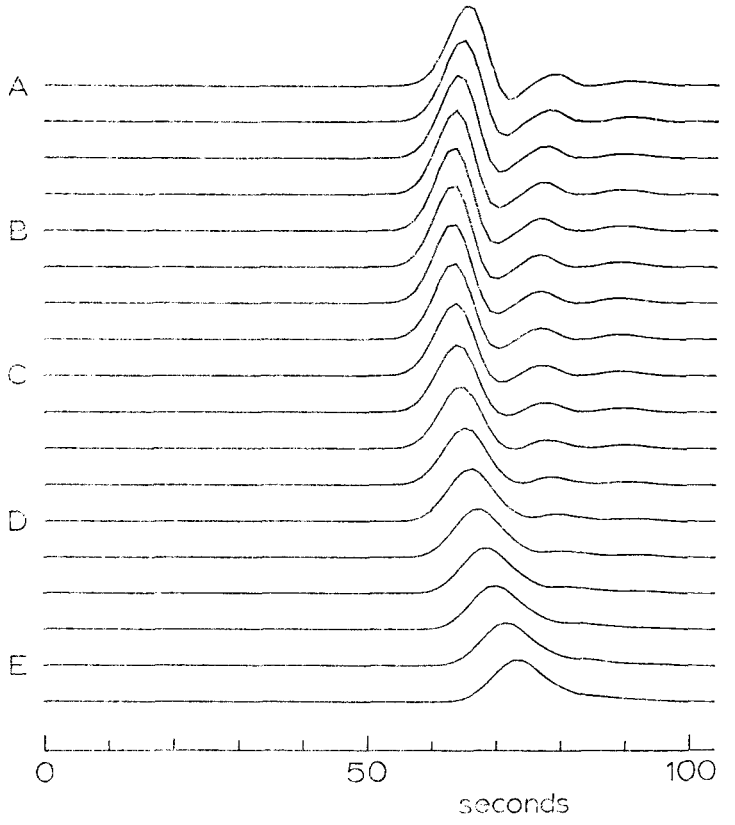

FIG. 11. Seismograms from an *SH* source 250 km deep, in a slab 50 km thick. Note the decrease in amplitude from A to E.

calculation using finite element models with different parameters indicates that the decrease in amplitude from A to E is accentuated by increasing the focal depth and by increasing the slab thickness. Investigations along these lines are continuing. Calculating the spectra of the observed traces allows comparison of amplitudes in the frequency domain. Such spectra are shown in Fig. 12. Amplitudes at zero frequency are very close to the geometrical spreading values for homogeneous material, inversely proportional to the distance from the source. At higher frequencies the effect of the slab becomes apparent.

In contemplating this technique to estimate slab structure, certain corrections would need to be applied. Accurate determination of the focal depth is necessary, before the finite element calculation can be made. A correction should be made for the two-dimensional radiation that has been assumed. A geometrical spreading correction, inversely proportional to the square of the distance from the focus, might be a good first approximation, provided that earthquake focus and seismograph are located in the same vertical plane, perpendicular to the arc. It may be necessary to incorporate the effects of damping. The earthquake radiation pattern should also be taken into account. The source used for the seismograms of Fig. 11 was a simple displacement *SH* pulse. Seismograms resulting from vertical and horizontal sources in the plane are shown in Fig. 13. The coda of each has had to be truncated because of contamination from high order reflections (Smith 1974), but the same amplitude variation as in Fig. 11 is apparent. A more complicated source, such as a double couple, could be used.

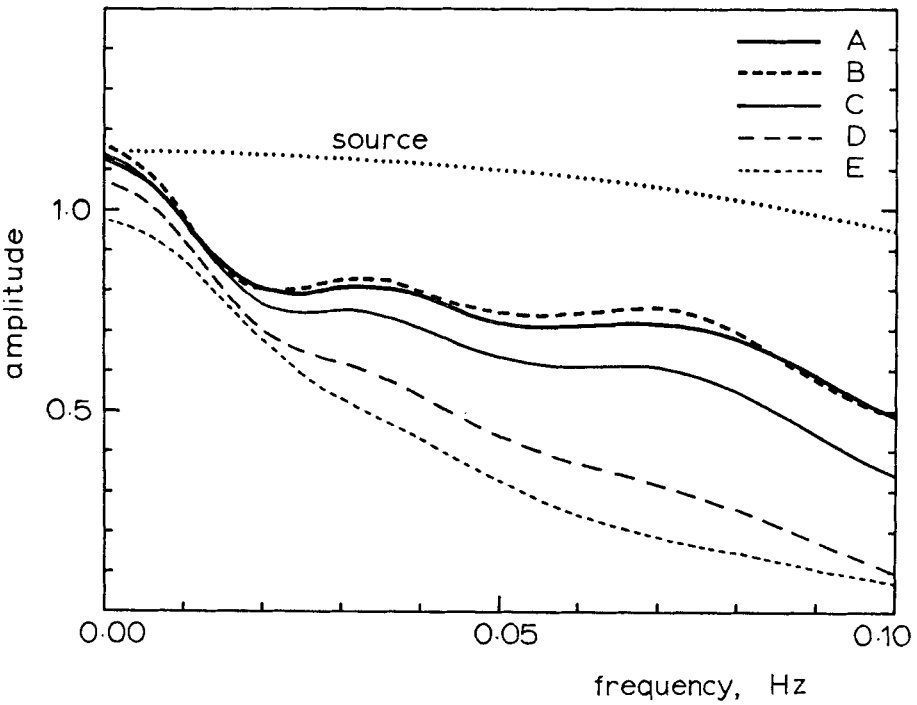

FIG. 12. Fourier spectra of representative seismograms from Fig. 11.

6. Conclusions

Seismic body wave propagation problems that have traditionally been treated by finite difference calculations can also be handled by the finite element method. It is a powerful tool for modelling the elastic behaviour of inhomogeneous media of irregular geometry. Damping may be included, but not all the features of the resulting attenuation are desirable, at least with currently available damping expressions. The use of a previously reported technique (Smith 1974) for eliminating reflections at the boundaries of a model greatly enhances the scope of numerical techniques for wave propagation problems. A general guiding rule for the design of a finite element mesh has been formulated, by examining the attenuation and dispersion which are inherent properties of the finite size of the elements. If the elements are nowhere larger than one eighth of the minimum wavelength of interest, attenuation and dispersion errors are kept to within a few per cent.

An attempt has been made to use the finite element method to reproduce Boore's (1972b) finite difference results for the amplification due to surface topography and Trifunac's (1971) analytical results for the effect of near-surface geology. Agreement with Boore's results is good, but in the latter case it is clear that a solution of longer duration is necessary. The numerical solution is unable, because of its finite duration, to reproduce accurately the sharp spectral peaks in the analytical result.

Calculations using a model of the New Zealand North Island seismic zone show that amplitudes of local earthquakes, observed at stations which ' look right down the slab ', are measurably reduced, at least at long periods. The amplitude variation across the top of the deep earthquake zone is dependent on focal depth and slab thickness. Finite elements can be used to model geophysical structures quite realistically. It is suggested that the modelling of a deep earthquake zone might lead

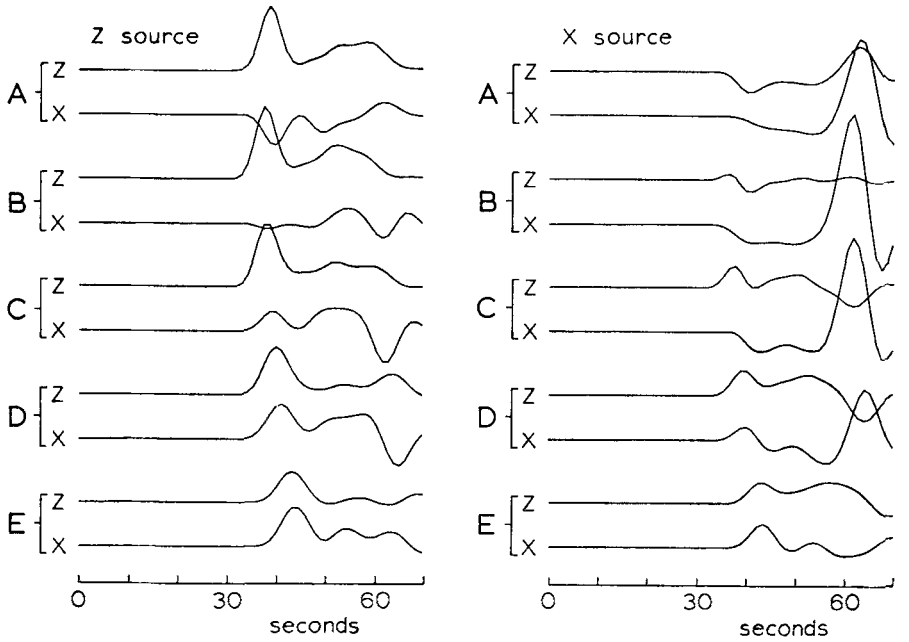

FIG. 13. Seismograms from a vertical source (left) and a horizontal source (right), written at the locations A to E. Two components are shown at each location. The same amplitude variation from A to E as in Fig. 11 is apparent.

to an inversion scheme whereby structural parameters such as the thickness of the dipping slab could be inferred.

Acknowledgments

I would like to express my appreciation to Professor B. A. Bolt for his many helpful comments and criticisms. My period of study in California was made possible by a New Zealand Postgraduate Research Fellowship. Computing was done on the CDC 6400 computer at the University of California. Berkeley, and also on the CDC 7600 computer at the Lawrence Berkeley Laboratory. Computing costs were met from National Science Foundation grants GI-34507 and GA-43310, and also from a grant from the Earthquake Engineering Research Center, University of California, Berkeley. I am also grateful to Mrs Augusta McClure, without whose co-operation in typing I should never have met publication deadlines.

Seismographic Station,
University of California,
Berkeley, California 94720.

References

Abramowitz, M. & Stegun, I. A., 1970. *Handbook of mathematical functions*, Dover Publications Inc., New York.

Alterman Z. & Karal, F. C., 1968. Propagation of elastic waves in layered media by finite difference methods, *Bull. seism. Soc. Am.*, **58**, 367–398.

Barazangi, M. & Isacks, B. L., 1971. Lateral variations of seismic-wave attenuation in the upper mantle above the inclined earthquake zone of the Tonga island arc: deep anomaly in the upper mantle, *J. geophys. Res.*, **76**, 8493–8516.

Boore, D. M., 1972a. Finite difference methods for seismic wave propagation in heterogeneous materials, in *Methods in computational physics*, Vol. 11, ed. B. A. Bolt, Academic Press, New York.

Boore, D. M., 1972b. A note on the effect of simple topography on seismic *SH* waves, *Bull. seism. Soc. Am.*, **62**, 275–284.

Boore, D. M., 1973. The effect of simple topography on seismic waves: implications for the accelerations recorded at Pacoima Dam, San Fernando Valley, California, *Bull. seism. Soc. Am.*, **63**, 1603–1609.

Carpenter, W. C. & Gill, P. A. T., 1973. Automated solutions of time dependent problems, *The mathematics of finite elements and applications*, 495, ed. J. R. Whiteman, Academic Press, New York.

Clough, R. W., 1971. Analysis of structural vibrations and dynamic response. *Recent advances in matrix methods in structural analysis and design*, Proceedings of U.S.–Japan seminar, August 1969. The University of Alabama Press, Huntsville, Alabama.

Courant, R., 1943. Variational methods for the solution of problems of equilibrium and vibrations, *Bull. Am. math. Soc.*, **49**, 1–23.

Davies, D. & McKenzie, D. P., 1969. Seismic travel-time residuals and plates, *Geophys. J. R. astr. Soc.*, **18**, 51–63.

Davis, L. L. & West, L. R., 1973. Observed effects of topography on ground motion, *Bull. seism. Soc. Am.*, **63**, 281–298.

Desai, C. S. & Abel, J. F., 1972. *Introduction to the finite element method*, Van Nostrand Reinhold, London.

Douglas, A., 1970. Finite elements for geological modelling, *Nature*, **226**, 630–631.

Drake, L. A., 1972a. Love and Rayleigh waves in nonhorizontally layered media, *Bull. seism. Soc. Am.*, **62**, 1241–1258.

Drake, L. A., 1972b. Rayleigh waves at a continental boundary by the finite element method, *Bull. seism. Soc. Am.*, **62**, 1259–1268.

Glover, P., McCowan, D. W. & Alexander, S. S., 1975. On computing displacement and stress fields from seismic sources in realistic geologic structures, *Geophys. J. R. astr. Soc.*, in press.

Gutenberg, B. & Richter, C. F., 1949. *Seismicity of the Earth*, Princeton University Press, Princeton, New Jersey.

Hamilton, R. M. & Gale, A., 1968. Seismicity and structure of North Island, New Zealand, *J. geophys. Res.*, **73**, 3859–3876.

Hatherton, T., 1970. Gravity, seismicity and tectonics of the North Island, New Zealand, *N.Z.J. Geol. Geophys.*, **13**, 126–144.

Jacob, K. H., 1972. Global tectonic implications of anomalous seismic *P* travel times from the nuclear explosion Longshot, *J. geophys. Res.* **77**, 2556–2573.

Kuhlemeyer, R. L. & Lysmer, J., 1973. Finite element accuracy for wave propagation problems (Technical note). *J. Soil Mech. Found. Div., Proc. ASCE*, **99**, SM5, 421–427.

Lysmer, J. & Drake, L. A., 1972. A finite element method for seismology. In *Methods in computational physics*. Vol. 11, ed. B. A. Bolt, Academic Press, New York.

Lysmer, J., Seed, H. B. & Schnabel, P. B., 1971. Influence of base-rock characteristics on ground response, *Bull. seism. Soc. Am.*, **61**, 1213–1231.

Mitronovas, W. & Isacks, B. L., 1971. Seismic velocity anomalies in the upper mantle beneath the Tonga-Kermadec island arc, *J. geophys. Res.*, **76**, 7154–7180.

Mooney, H. M., 1970a. Upper mantle inhomogeneity beneath New Zealand: seismic evidence, *J. geophys. Res.*, **75**, 285–309.

Mooney, H. M., 1970b. Theoretical and observed travel times for New Zealand deep earthquakes, *N.Z.J. Geol. Geophys.*, **13**, 703–717.

Newmark, N. M., 1959. A method of computation for structural dynamics. *Proc. Am. Soc. Civ. Eng., J. Eng. Mech. Div.*, **85**, EM3, 67–94.

Norrie, D. H. & de Vries, G., 1973. *The finite element method. Fundamentals and applications*, Academic Press, New York.
Oliver, J. & Isacks, B. L., 1967. Deep earthquake zones, anomalous structures in the upper mantle, and the lithosphere, *J. geophys. Res.*, **72,** 4259–4275.
Reimer, R. B., 1973. *Deconvolution of seismic response for linear systems*, PhD Thesis, College of Engineering, University of California, Berkeley.
Rogers, A. M., Katz, L. J. & Bennett, T. J., 1974. Topographic effects on ground motion for incident *P* waves: a model study, *Bull. seism. Soc. Am.*, **64,** 437–456.
Shipley, S. A., Leistner, H. G. & Jones, R. E., 1967. Elastic wave propagation—a comparison between finite element predictions and exact solutions. *Proceedings, International symposium on wave propagation and dynamic properties of earth materials*, 509–519. University of New Mexico Press, Albuquerque.
Smith, W. D., 1973. Upper mantle velocities determined from local observations of deep earthquakes, *Bull. seism. Soc. Am.*, **63,** 807–817.
Smith, W. D., 1974. A nonreflecting plane boundary for wave propagation problems, *J. comp. Phys.*, **15,** 492–503.
Trifunac, M. D., 1971. Surface motion of a semi-cylindrical alluvial valley for incident plane *SH* waves, *Bull. seism. Soc. Am.*, **61,** 1755–1770.
Trifunac, M. D., 1972. Erratum to 'Surface motion of a semi-cylindrical alluvial valley for incident plane *SH* waves', *Bull. seism. Soc. Am.*, **62,** 666.
Wilson, E. L., 1969. Elastic dynamic response of axisymmetric structures. *Structures and materials research*, Report 69–2, College of Engineering, University of California, Berkeley.
Wyss, M., 1973. The thickness of deep seismic zones, *Nature*, **242,** 255.
Zienkiewicz, O. C., 1971. *The finite element method in Engineering Science*, McGraw–Hill, Maidenhead.

Appendix

Computing notes

Programs have been written in FORTRAN for the CDC 7600 computer at the Lawrence Berkeley Laboratory, one for *SH* propagation (SHIMP) and one for *P* and *SV* (SVIMP). Both can accommodate models of up to 5000 nodes, in two dimensions. Cartesian coordinates have been used throughout. Considerable flexibility has been built into the subroutine that sets up the model geometry, in order to minimize the effort involved in preparing the data.

Storage of the stiffness matrix is always a critical factor in finite element work. At first glance it might seem that for 5000 nodes, and two displacement components at each node, the matrix will have 10^4 rows and columns, and will thus require 10^8 words of storage. But such is not the case. The matrix is symmetric and very sparse, and is often stored in banded form. But if an explicit algorithm is used, such as Runge-Kutta, the storage requirements can be reduced even more.

For a rectangular two-dimensional grid, there are never more than eight nodes adjacent to a given node. So in the *SH* case the stiffness matrix never has more than nine non-zero terms in any one row. With irregular grids there may be more than nine terms, and I have allowed up to eleven. So all that is necessary is to store these non-zero terms, with another matrix to indicate to which columns these terms belong. Let us call this second matrix the 'reference' matrix. Storage requirements for the stiffness matrix are thus reduced to 11×5000 in the *SH* case, and $22 \times 10\,000$ in the *P-SV* case, together with 11×5000 for the reference matrix, in both cases.

A further reduction is possible. In areas of the grid where the elements are regular and the material homogeneous, the stiffness relationships of each node to its

neighbours will be identical. This is, the rows of the stiffness matrix, packed in the form outlined above, will be identical, and there is thus no need to duplicate storage. Rather, all that is needed is a pointer to indicate, given a particular node, in which row of the condensed stiffness matrix the appropriate stiffness terms are to be found. The reference matrix retains its full form.

I have therefore allowed only 11×1000 words for the *SH* stiffness matrix, and 22×2000 for *P–SV*. This storage is available in core in the CDC 7600 computer. 1000 was a somewhat arbitrary choice; it could have been reduced further. Having specified the nodal co-ordinates and element connections, all that is necessary in setting up the model is to indicate which nodes will have identical stiffness relations with their neighbours. If the model has less than 1000 nodes, the option need not be used.

The identical technique applies to the damping matrix, if it is used. The same reference matrix and pointer vector apply to the damping matrix as to the stiffness matrix, so the extra storage that is needed is 11×1000 for *SH* and 22×2000 for *P–SV*. A simple subroutine which multiplies the packed matrices by vectors has been written, to facilitate matrix arithmetic.

It should be emphasized that this condensed storage configuration is only possible because the algorithm used is an explicit one. If an implicit scheme were used, storage of at least the stiffness matrix would have to be in banded form. This represents a considerable increase in storage requirements, as well as significantly more work in preparing the data because efforts should be made to achieve minimum bandwidth. The bandwidth of the matrix is immaterial for the condensed storage configuration that has been used.